Bimetallic nanoparticles: A single step synthesis, stabilization, and characterization of Au–Ag, Au–Pd, and Au–Pt in sol–gel derived silicates

Supriya Devarajan [a], Parthasarathi Bera [b], S. Sampath [a,*]

[a] *Department of Inorganic and Physical Chemistry, Indian Institute of Science, Bangalore 560 012, India*
[b] *Solid State and Structural Chemistry Unit, Indian Institute of Science, Bangalore 560 012, India*

Abstract

Nanobimetallic particles consisting of Au–Pd, Au–Ag, and Au–Pt have been synthesized in a single step by a sol–gel process and stabilized in liquid and solid matrices. Organically modified silicates (Ormosils) that play a dual role of a matrix and of a stabilizer have been used to obtain very stable dispersions in the form of sols, gels, and monoliths. The simultaneous reduction of metal ions leads to either a surface enriched with one component or an alloy type of structure depending on the bimetal combination. The nanometallic dispersions are characterized by absorbance, TEM, XRD, IR, XPS, and CO adsorption studies. The stabilized nanoparticles are found to be good electrocatalysts and the preliminary results on the electrochemical reduction of oxygen are reported.

Keywords: Bimetallic nanoparticles; Sol–gel; Au; Ag; Pd; Pt; Aminosilane

1. Introduction

Bimetallic nanoparticles are of wide interest since they lead to many interesting size-dependent electrical, chemical, and optical properties. They are particularly important in the field of catalysis since they often exhibit better catalytic properties than their monometallic counterparts [1–5]. Gold is very useful as an alloying metal due to its relatively low reactivity. It has been used in conjunction with metals such as palladium [2,3,6–18] and platinum [5,9,14,19–23] for various catalytic reactions. The structure of bimetallic combinations depends mainly on the preparation conditions and the miscibility of the two components. Combinations such as Au–Pd and Au–Pt have been reported to exhibit a core–shell structure while Au–Ag forms either a core–shell [24–26] or an alloy [23,27–39] phase depending on the preparation conditions.

Among the bimetallics, Au–Pd is one of the combinations that has been extensively studied in terms of preparation, stabilization, and catalytic activity. Turkevich and Kim have studied the morphology of Au–Pd bimetallic particles, prepared by using hydroxylamine hydrochloride as a reducing agent [6]. Preparation of core–shell type nanostructures has been demonstrated by the successive formation of bimetallic Au–Pd colloids in which a core of one metal is encapsulated by a shell of another [9,11,12]. In certain cases, successive reductions yielded a cluster-in-cluster structure or mixtures of monometallic components [13]. Simultaneous reduction of the metal ions [14–16] using polymers as stabilizers produced Au core–Pd shell structured particles. Liu and co-workers have reported the formation of Au-core–Pd-rich-shell type structures by a simultaneous alcohol reduction method [17]. Guczi and co-workers prepared 4–7 nm sized Au–Pd bimetallic particles in aqueous media by the simultaneous addition of a mixture of trisodium citrate (reducing agent) and tannin (stabilizing agent) to the metal ions. This hydrosol deposited on a TiO_2 support has been shown to be catalytically very active toward CO oxidation [18].

* Corresponding author.
E-mail address: sampath@ipc.iisc.ernet.in (S. Sampath).

As for the combination Au–Pt, Toshima and co-workers have used a strategy similar to the synthesis of Au–Pd bimetallic particles to obtain Au core–Pt shell type structures [5,14]. The polymer-protected particles have been used as catalysts for visible-light-induced hydrogen evolution reaction. Flynn and Gewirth prepared Au–Pt core–shell nanoparticles by first reducing Au^{3+} and subsequently reducing tetrachloroplatinate ion on the gold particles [19]. The bimetallic sol has been used as substrates for surface-enhanced Raman scattering (SERS) studies [19,20]. Liz-Marzan and Philipse have used optically transparent imogolite fibers to stabilize Au–Pt, Au–Ag, and Ag–Pt bimetallic hydrosols. The reduction carried out using $NaBH_4$, has been reported to yield very stable particles 2–3 nm in size [23].

Both Au and Ag have very similar lattice constants and are completely miscible over the entire composition range [38]. Hence, single-phase alloys can be achieved at any desired composition. The reports describing the synthesis of Au–Ag alloy clusters [23,27–39] could be categorized into two broad methods involving a top-down approach from a bulk alloy using an evaporation and condensation process [27] or reduction of metal ions in a suitable environment [23,28–39]. Esumi and co-workers have prepared Au–Ag alloy phases in laponite suspensions [28]. Shi and co-workers have reported the formation of Au–Ag alloy nanoparticles in monolithic mesoporous silica where amino groups are used to stabilize the alloy particles [29]. Monolayer-protected alloy clusters have been synthesized using a modified Brust's synthesis procedure [30,31,36,37]. A simple co-reduction of $HAuCl_4$ and $AgNO_3$ with sodium citrate in aqueous solution is reported to yield 17–22 nm sized alloy particles [38]. We have recently prepared mercaptopropionate-stabilized Au–Ag alloy hydrosols and demonstrated its phase transfer from the aqueous to an organic phase [39].

Most of the reported literature on bimetallic particles, however, concerns the stabilization of metallic particles in aqueous media in the presence of surfactants or water-soluble polymers as stabilizers. It is desirable to have the flexibility of using nanoparticles both in the liquid and solid phases, preferably with the same matrix and stabilizer. Stabilization in a solid matrix avoids coagulation and precipitation of particles. This would facilitate the studies involving nanoparticles on solid matrices. Additionally, the bimetallic catalysts can be recovered easily after the reaction and hence elaborate separation procedures are avoided. Lev and co-workers [40] proposed the use of functionalized silicate matrices to stabilize monometallic particles such as gold and palladium. Preparation and stabilization of bimetallic/alloy particles in silicate matrices have the advantages of a single step preparation procedure, very uniform distribution of nanometer sized particles and the versatility of making the matrix in the form of sols, gels, films and monoliths. We have extended the method of Lev and co-workers [40] to stabilize bimetallic systems [41]. The sol–gel processing of materials coupled with the inherent advantages of the organically modified silicates (Ormosils) make these matrices very attractive as supports and stabilizers for nanometallic particles in both liquid and solid phases. We have been able to synthesize a range of nanobimetallic combinations such as Au–Pd, Au–Ag, Au–Pt, and Ag–Pt. The present paper details the preparation and characterization of Au–Pd, Au–Ag, and Au–Pt bimetallic particles. The sol–gel stabilized particles are characterized by various techniques and the films containing these particles are used for preliminary studies on the electrocatalytic reduction of oxygen.

2. Experimental

2.1. Materials

N,*N*′-[3-(trimethoxysilyl)propyl]diethylenetriamine (TPDT) was the product of Aldrich, USA. Tetraethoxysilane (TEOS) was obtained from Chemplast, Sanmar, India. Chloroauric acid, palladium chloride, silver nitrate, chloroplatinic acid, sodium borohydride, methanol, and all other chemicals used were of analytical grade. Double-distilled water was used in all the experiments. Glassy carbon electrodes polished to a mirror finish with varying grades of alumina powder were used to carry out electrochemistry experiments.

2.2. Apparatus

UV–vis spectra were recorded using a Hitachi 3000 spectrophotometer. The samples were in the form of sols, thin films, and gels. High-resolution TEM measurements were carried out using a JEOL 3010 Model, operating at 300 kV. Samples were prepared by placing a drop of the sol on a copper grid and allowing the solvent to evaporate. FT-IR experiments were carried out on a Bruker Equinox 55 spectrophotometer. The samples for CO adsorption studies were prepared by purging the sols containing the desired metal particles with gaseous CO for several minutes followed by equilibration. A few drops of the sol were placed on a KBr pellet and allowed to dry before IR spectra were recorded. Powder X-ray analysis was carried out using a Philips Model PW 1050/37 diffractometer, operating at 40 kV and 30 mA, with a step size of 0.02° (2θ). Dried and powdered samples of colloids with the stabilizer before and after heat treatment were used for the measurements. XPS of Au–Pd, Au–Ag, and Au–Pt bimetallic clusters were recorded on an ESCA-3 Mark II spectrometer (VG Scientific Ltd., England) using Al$K\alpha$ radiation (1486.6 eV). The samples for XPS analysis were pellets of 8 mm diameter and were degassed initially for 5 h. The samples were then placed into an ultra-high-vacuum (UHV) chamber at 10^{-9} Torr for analysis. The binding energies were calculated with respect to C(1s) at 285 eV.

2.3. Preparation of bimetallic dispersions

The preparation of bimetallic particles was carried out as follows: 130 µl of N,N'-[3-(trimethoxysilyl)propyl]diethylenetriamine (TPDT) was added to 3.8 ml of methanol followed by 50 µl of H_2O and 50 µl of 0.1 M HCl. This mixture was shaken well for a couple of minutes. Different volumes of 0.01 M $AuCl_3$ and 0.01 M $PdCl_2$/$AgNO_3$/H_2PtCl_6 were then added to the silica sol and mixed well until the solution became homogeneous. Sodium borohydride (0.0025 g) was then added with vigorous stirring. Instantaneous color change ranging from deep violet of Au colloid to the brown color of Pd and Pt or yellowish brown in the case of Ag colloid, depending on the composition, was observed. Different compositions ranging from 100:0.25 to 100:5 molar ratio of the silane precursor to the metal salt could be prepared without any precipitation. Various molar compositions of the two metal components such as 0.25:0.75, 0.43:0.57, 0.5:0.5, 0.57:0.43, 0.75:0.25, and 0.9:0.1 were prepared using the same protocol. The sols and the resulting solid monoliths for all the compositions were very stable over extended periods of several months.

2.4. Preparation of thin films, gels, and thick films

Films of different thickness ranging from 0.1 to 10 µm could be cast on glass slides by a coating process. Gels and monoliths of any desired shape were obtained by allowing the solvent to evaporate. The dried material was found to shrink considerably but slow evaporation of the solvent led to crack free monoliths. For electrochemistry experiments, a mixture of TPDT and TEOS was copolymerized in the ratio 3:1 and used as a stabilizer for the metallic nanoparticles. This was essential to accelerate the condensation and subsequent drying of the cast film. A drop of this sol was placed on a glassy carbon surface and the solvent was allowed to evaporate. The film was heated to 125 °C for 12 h to improve the cross-linking and subsequently used for cyclic voltammetry experiments.

3. Results and discussion

The sol–gel derived silicates containing the nanoparticles are very stable, both in the liquid phase and solid phase. The stability is checked by following the absorbance spectra over extended periods of several months. The gels are clear and transparent, though colored to different extent depending on the composition of the bimetal. The amino groups present in the silicate stabilize the bimetallic nanoparticles as proposed by Lev and co-workers for the monometals [40]. The particle size distribution is fairly uniform as will be shown later. The use of sodium borohydride results in a fast reduction of metal ions.

3.1. UV–visible spectral studies

3.1.1. Au–Pd

The absorbance spectra of the sols containing various compositions of the metal components (0.5:0.5, 0.75:0.25, and 0.9:0.1 molar ratios of $AuCl_3$:$PdCl_2$, respectively) are given in Fig. 1. The molar ratio of silane to metal salts is maintained constant at 100:0.5. The absorbance studies have been carried out after ensuring complete reduction of the metal ions based on the kinetics of reduction of individual metal ions. Absorbance spectra corresponding to the monometallic components are also given for comparison. The absence of peaks at 310 nm characteristic of unreduced Au(III) and at 440 and 325 nm characteristic of unreduced Pd(II) indicates complete reduction of the metal ions. The spectrum of Au monometal (Fig. 1, inset, g) shows a characteristic surface plasmon at 520 nm and the sol has a deep wine red color. The palladium sol shows broad absorption (Fig. 1, inset, f) over the entire range and is brown in color [15]. The absorbance behavior of the bimetallic dispersions is found to be different from that of the monometallic components. These are similar to the spectra reported for Au–Pd bimetallic systems by Toshima and co-workers [16] suggesting that bimetallic particles are formed in silicate matrices as well. In order to confirm the bimetallic nature of the particles, a physical mixture is prepared from the already prepared individual components and its absorbance is compared to that of the bimetallic Au–Pd colloid of the same composition (Fig. 1, inset, d and e). The absorbance band characteristic of gold that appears at 520 nm is absent in the case of the bimetal while it is present in the case of the physical mixture. A bimetallic sol containing less than 50% of gold does not have a characteristic absorption band due to gold clusters and the color of the sol is brown. This clearly

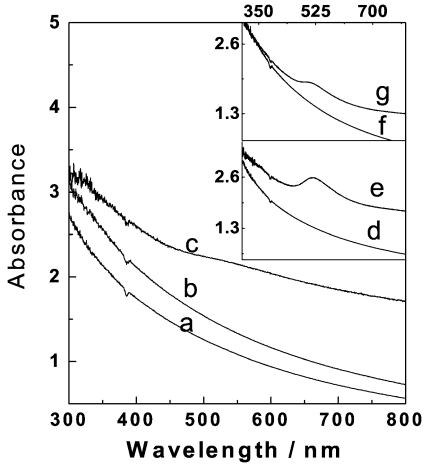

Fig. 1. Absorbance spectra of TPDT-stabilized Au–Pd sol: (a), (b), and (c) correspond to Au–Pd bimetallic colloids of molar ratios 0.5:0.5, 0.75:0.25, and 0.9:0.1 of the Au and Pd salts, respectively. Inset: (d) 0.5:0.5 of Au/Pd sol; (e) physical mixture of same composition. Inset: (f) Pd and (g) Au sol. The molar ratio of the silane to metal salts of Au and Pd is 100:0.5:0.5, respectively.

indicates that dispersions of Au–Pd bimetallic systems do not contain Au monometallic clusters but clusters with bielemental structure. The change in the absorbance spectra of the bimetallic colloid from that of the individual components can be primarily attributed to the change in the dielectric function with mixing of different metal atoms [42].

3.1.2. Au–Pt

The UV–vis spectra of Au–Pt sol are very similar to that of Au–Pd sol. Fig. 2 shows the comparison between the UV–vis spectra of different compositions of Au and Pt (0.75:0.25, 0.5:0.5, and 0.25:0.75 molar ratios of $HAuCl_4$:H_2PtCl_6) and the monometals. The molar ratio of silane to metal ion is 100:0.25. This is less than the corresponding ratios used for other systems. It is known that Au and Pt tend to precipitate when mixed together at high concentrations of Pt [14]. The Pt sol is brown and shows a broad absorption band. The absence of peaks at 378 and 460 nm indicates the reduction of Pt(IV). However, a shoulder is observed close to 350 nm. The origin of this band is not clear but it is speculated to be due to the unreduced complex. Like Au–Pd bimetals, the surface plasmon of Au gets completely suppressed when the Pt component is higher than 50%, thus indicating the formation of bimetallic structure. This is supported by the XPS studies as will be shown later. In the case of physical mixtures, the plasmon is clearly visible for all ratios of Au and Pt (Fig. 2, inset, f).

3.1.3. Au–Ag

The UV–vis spectra of Au–Ag bimetals are quite different from Au–Pd and Au–Pt bimetals. This combination is known to form alloys when reduced simultaneously. Fig. 3A shows the absorption spectra of different compositions of Au and Ag (0.57:0.43, 0.43:0.57, and 0.25:0.75 molar ratios of $HAuCl_4$:$AgNO_3$) along with the monometals. The molar ratio of silane to metal is 100:0.5. Alloy formation is confirmed by the optical absorption spectra that show only one surface plasmon peak and the position of the λ_{max} depends on the composition. The plasmon band blue-shifts with increasing amount of silver and is similar to the observations reported earlier [38]. The absorption spectra of Au, Ag, and Au–Ag alloy nanoparticles of varying mole fractions show a linear relationship between the λ_{max} and Au mole fraction (Fig. 3B). A physical mixture of the individual colloids, however, shows two surface plasmon peaks corresponding to the monometallic counterparts (Fig. 3, inset, f). The stability of the silver colloids in the silicate matrix, however, is very low. This could be attributed in part to the low stability constant of the Ag–amine complex [40,43,44]. This is subsequently revealed in the relative instability of Au–Ag alloys where the Ag content is higher than 50%.

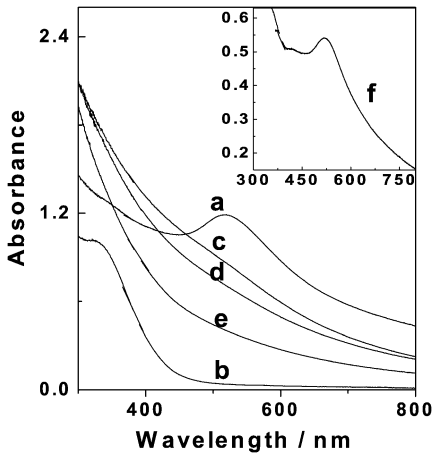

Fig. 2. Absorbance spectra of TPDT-stabilized Au–Pt sol: (a) and (b) correspond to Au and Pt colloids; (c), (d), and (e) correspond to Au–Pt bimetallic colloids of molar ratios 0.75:0.25, 0.5:0.5, and 0.25:0.75 of the Au and Pt salts, respectively. Inset: (f) physical mixture of molar ratio 0.5:0.5. The molar ratio of the silane to metal salts of Au and Pt is 100:0.25:0.25, respectively.

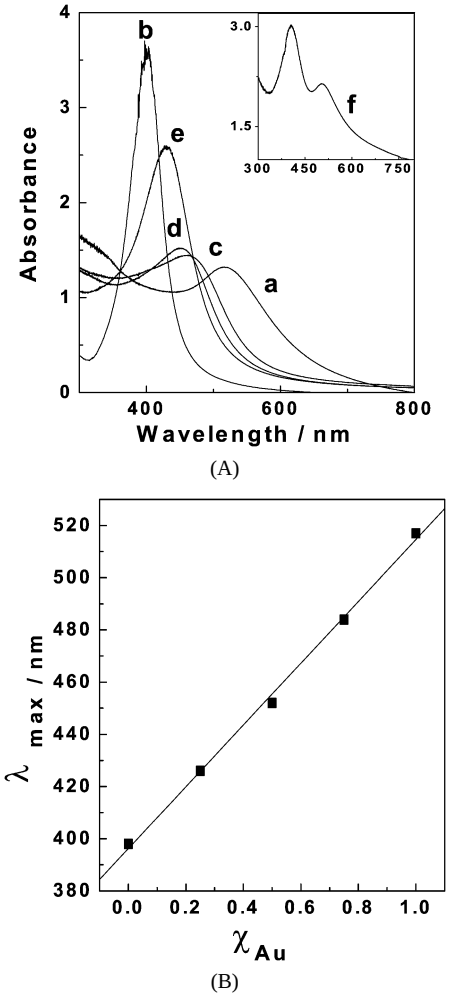

(A)

(B)

Fig. 3. (A) Absorbance spectra of TPDT-stabilized Au–Ag sol: (a) and (b) correspond to Au and Ag colloids; (c), (d), and (e) correspond to Au–Ag bimetallic colloids of molar ratios 0.57:0.43, 0.43:0.57, and 0.25:0.75 of the Au and Ag salts, respectively. Inset: (f) physical mixture of molar ratio 0.5:0.5. The molar ratio of the silane to metal salts of Au and Ag is 100:0.5:0.5, respectively. (B) Variation of surface plasmon band with the alloy composition.

The formation of bimetallic dispersions depends on the kinetics and thermodynamics of reduction of individual components. The complete reduction of Au(III), Ag(I), Pd(II), and Pt(IV) under the present conditions requires 3, 5, 10, and 25 min, respectively. The stability constants associated with the Ag(en), Pd(en), and Pt(en) complexes are $10^{7.4}$, $10^{26.9}$, and $10^{36.5}$, respectively [40,43,44]. The value for Au(en) is expected to be close to that of silver based on the ease of reduction as observed in the time required for complete formation of the metallic colloid. Hence, it is expected that Pd and Pt may form a shell, while Au may form the core of the bimetal in the case of Au–Pd and Au–Pt bimetallic structures. However, from the XPS studies and CO adsorption measurements, it is observed that both the metals are present with an enrichment of Pt and Pd on the surface. In the case of Au–Ag bimetal, silver enrichment is observed. It is reported that planar Au–Ag alloys formed by high-temperature method exhibit an enrichment of Ag on the surface, due to the lower heat of sublimation of Ag than Au [45]. However, in the case of preparation of nanoparticles under ambient conditions, the borohydride reduction and the metal atom deposition chemistry may also play a role in determining the surface enrichment.

The stability of the bimetallic particles in the TPDT matrix is primarily attributed to the presence of both Si–OH and $–NH_2$ groups. It is found that the use of only tetraethoxysilane or methyltrimethoxysilane or trimethylamine as the stabilizer results in the precipitation of the particles. This suggests a dual role for the aminosilanes as stabilizers of nanobimetallic particles. It is possible that the amino groups stabilize the nanobimetallic particles while the –Si–O–Si– and Si–OH form a network surrounding the metallic particles. Additionally, the use of long-alkyl-chain-containing matrices is expected to help in the stabilization of the nanoparticles by keeping them far apart and thereby preventing coagulation. The formation of silica shell around metal particle where silanes are used for stabilization is already known in the literature. Mulvaney and co-workers [46] have reported the formation of silica shells around gold nanoparticles prepared using silanes. Lev and co-workers [40] postulated that silanes form a network around the nanometallic particles of gold, silver, platinum, and palladium.

The stability of the mono- as well as the bimetallic colloidal dispersions is found to be very good and the particle size does not change with time. Absorbance of the sol as well as the dry gel is found to be indistinguishable immediately after preparation and after several months of storage. The particle size distribution is retained in both solid and liquid phases. It is observed that the absorbance spectra of a silicate film (3-μm thickness) containing nanobimetallic particles of composition 1:1 molar ratio of the salts is nearly the same as that of the sol. In this case, the film is formed from a mixture of TPDT and TEOS. The addition of TEOS to the sol decreases the cross-linking time but does not change the absorbance spectra.

3.2. TEM studies

3.2.1. Au–Pd

TEM images indicate that the particles are nearly spherical (Fig. 4a) and the average particle size ranges between 2 and 7.5 nm with the maximum close to 3.5 nm. This is shown in the histogram of particle size distribution (Fig. 4c). The uniform distribution of these particles combined with their small size leads to a good catalyst as exemplified in the use of these materials for the electrocatalysis of oxygen reduction. The (111) lattice (Fig. 4b) spacing is determined to be 2.34 ± 0.01 Å. Bulk Au and Pd have lattice spacings of 2.36 (JCPDS 4-0784) and 2.25 (JCPDS 5-0681), respectively.

3.2.2. Au–Pt

The size of Au–Pt bimetallic particle varies between 1 and 6 nm (Figs. 5a, 5c). Fig. 5b shows the HRTEM of the bimetallic particles. The lattice is quite well-resolved and equally spaced showing the single crystalline nature of the nanoparticle. The lattice spacing is 2.30 ± 0.01 Å. Bulk Pt has a lattice spacing of 2.27 Å (JCPDS 4-0802). Assuming Vegard's law behavior, the observed lattice spacing will yield a nominal composition of 1:2 Au/Pt for a starting composition of 5:1 Au/Pt. This value should be treated with some caution since even a small variation in the measurement of the lattice spacing could lead to a large error in the final composition.

3.2.3. Au–Ag

Au–Ag alloy particle size ranges from 1 to 6 nm (Fig. 6a) with the maximum close to 2.5 nm as can be seen from the histogram in Fig. 6c. The lattice spacing obtained from the HRTEM (Fig. 6b) is 2.30 ± 0.01 Å. There is no lattice mismatch observed since the Au and Ag have very similar lattice parameters (JCPDS 4-0783, JCPDS 4-0784).

3.3. XRD studies

The diffractograms of the bimetallic combinations generally show broad bands while their monometallic counterparts exhibit fairly sharp bands. The particle sizes of the bimetallic combinations determined from the XRD spectra correlate well with the sizes obtained from TEM measurements. The particle size is calculated based on the Scherrer equation:

$$t = \frac{0.9\lambda}{B\cos\theta}, \tag{1}$$

where t corresponds to the particle size in Å, λ is the X-ray wavelength, θ is the Bragg angle, and B corresponds to the full width at half maximum (fwhm, in radians) of the peak under consideration. When the samples are heated to 200 °C for 3 h, the peaks become well-defined and sharp due to increased crystallinity (not shown). On heat treatment the particle size increases threefold for all bimetallic combinations.

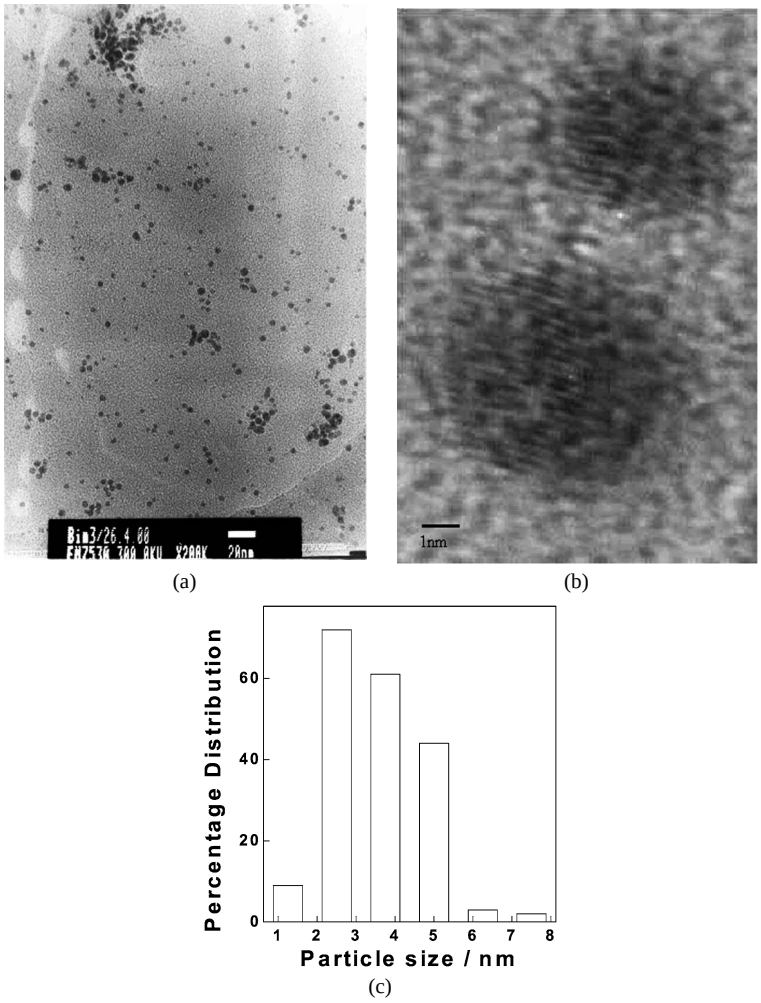

Fig. 4. TEM picture of the TPDT-stabilized Au–Pd bimetallic colloid. The molar ratios of silane to metal salts is 100:5:5. (a) Bar indicates 20 nm; (b) HRTEM image, bar indicates 1 nm; (c) particle size distribution.

3.3.1. Au–Pd

The XRD spectra of the monometals as well as the bimetal of different compositions have been recorded for the as-prepared samples in the form of dry powders (Fig. 7A, a–c). The molar ratio of silane to metal salt is maintained at 100:5. As for the monometals, it is observed that Pd is more crystalline than the gold nanoclusters in silicate matrices. The peak that appears at around 38° (2θ) corresponds to the (111) crystallographic plane and the peak at around 45° (2θ) corresponds to the (200) plane (JCPDS 4-0784, 5-0681). The diffractograms show that (111) crystallographic surface is marked for gold clusters ($2\theta = 38.46°$) and is broad, while the (200) plane is less distinct ($2\theta = 44.41°$) (Fig. 7A, a). Two additional broad bands are observed at 64.48° (2θ) and 77.71° (2θ) and they correspond to the (220) and (311) planes of Au, respectively.

In the case of Pd, there is a strong band at 56.33° (2θ), which closely matches the (222) plane of PdO (JCPDS 46-1211). This is not surprising since it is known that Pd gets oxidized fairly fast when under ambient conditions. Another strong band is seen at 45.37° (2θ), which corresponds to the (200) plane of Pd.

The observed reflections for the bimetal clusters are slightly different from that of the monometallic components. The (111) plane is observed at 38.62° (2θ) and the (200) plane occurs at a value of 45.25° (2θ) for the bimetal of molar ratio 1:1 (Fig. 7A, b). These values lie in between the values reported for monometallic clusters. The particle size has been calculated (using Eq. (1)) to be 4 ± 1 nm based on the (111) peak. These values are close to the values deduced from TEM measurements. A fairly strong band is seen at 66.2° (2θ), which lies close to the (400) reflection of PdO. Two sharp bands are seen at 75.34° (2θ) and 75.15° (2θ) in Au–Pd bimetal and Pd, respectively. This most likely corresponds to the (420) plane of the oxide.

3.3.2. Au–Pt

The molar ratio of silane to metal salt is maintained at 100:5, while the ratio of Au/Pt is maintained at 5:1 in order to avoid precipitation. Pt, like Pd is more crystalline than gold nanoclusters in silicate matrices (Fig. 7B, e). The (200) band is very sharp and is observed at 45.44° (2θ) (JCPDS 4-0802). A strong band is observed at 56.47° (2θ) that appears to be due to the (102) reflection of PtO_2 (JCPDS 38-1355).

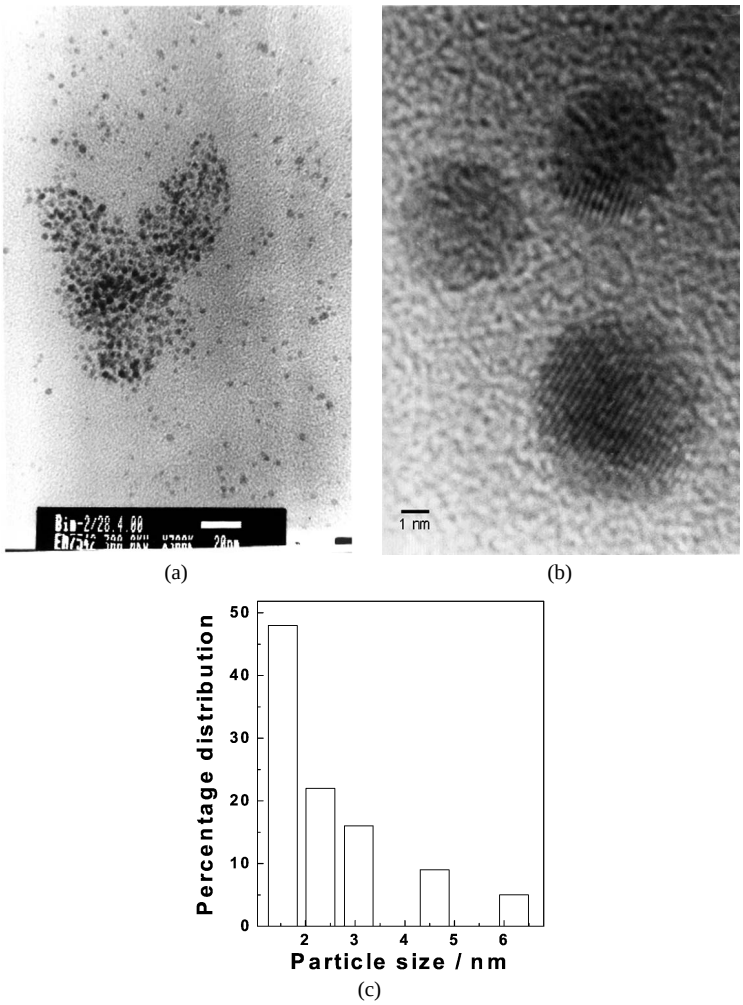

(a) (b) (c)

Fig. 5. TEM picture of the TPDT-stabilized Au–Pt bimetallic colloid. The molar ratios of silane to metal salts is 100:5:1. (a) Bar indicates 20 nm; (b) HRTEM image, bar indicates 1 nm; (c) particle size distribution.

Bands are also observed at 65.94° (2θ) and 75.22° (2θ) that correspond to the (111) and (201) planes of PtO_2, respectively (JCPDS 38-1355). The XPS data of the bimetal also shows Pt in oxidized states.

The Au–Pt bimetal exhibits a broad band at 38.35° (2θ) that corresponds to the (111) plane (Fig. 7B, d). There is a broad peak at 44.58° (2θ) and is attributed to the (200) plane. Two additional bands are observed at 65° and 77.73° (2θ) that correspond to PtO_2 (JCPDS 38-1355). The particle size is calculated to be 7 ± 1 nm based on Eq. (1) using the (111) peak and is close to the particle size observed by TEM measurements.

3.3.3. Au–Ag

As mentioned in the Introduction, Au and Ag have very similar lattice constants and hence their d-values and 2θ values lie very close to each other (JCPDS 4-0783, 4-0784). Fig. 7C (g and f) shows the XRD spectra corresponding to Ag and the Au–Ag alloy, respectively. The molar ratio of silane to metal salt is maintained at 100:5, while the ratio of Au:Ag is 1:1. As for the diffractogram of Ag, the strongest band is observed at 38.14° (2θ) that corresponds to the (111) plane. A broad band is observed at 44.15° (2θ) that can be attributed to the (200) crystallographic plane. Two broad reflections are observed at 64.55° and 77.48° (2θ) that correspond to the (220) and (311) planes. In the case of the Au–Ag alloy (Fig. 7C, f), all reflections are similar to monometallic Au and Ag. The particle size is calculated to be 5 ± 1 nm based on Eq. (1) using the (111) peak, which corroborates well with the data obtained from TEM.

3.4. XPS studies

3.4.1. Au–Pd

The as-prepared sample does not show any signal for Au($4f$) or Pd($3d$) in the XPS spectra. After the sample was etched for about 10 min peaks start to appear. Fig. 8A shows the Au($4f_{7/2,5/2}$) region after 10 min of etching. The signals appearing at 83.9 and 88.0 eV are assigned to Au^0. During the course of etching, the intensity of Au($4f$) increases. Another broad signal appears in the region 333.0–340 eV and is

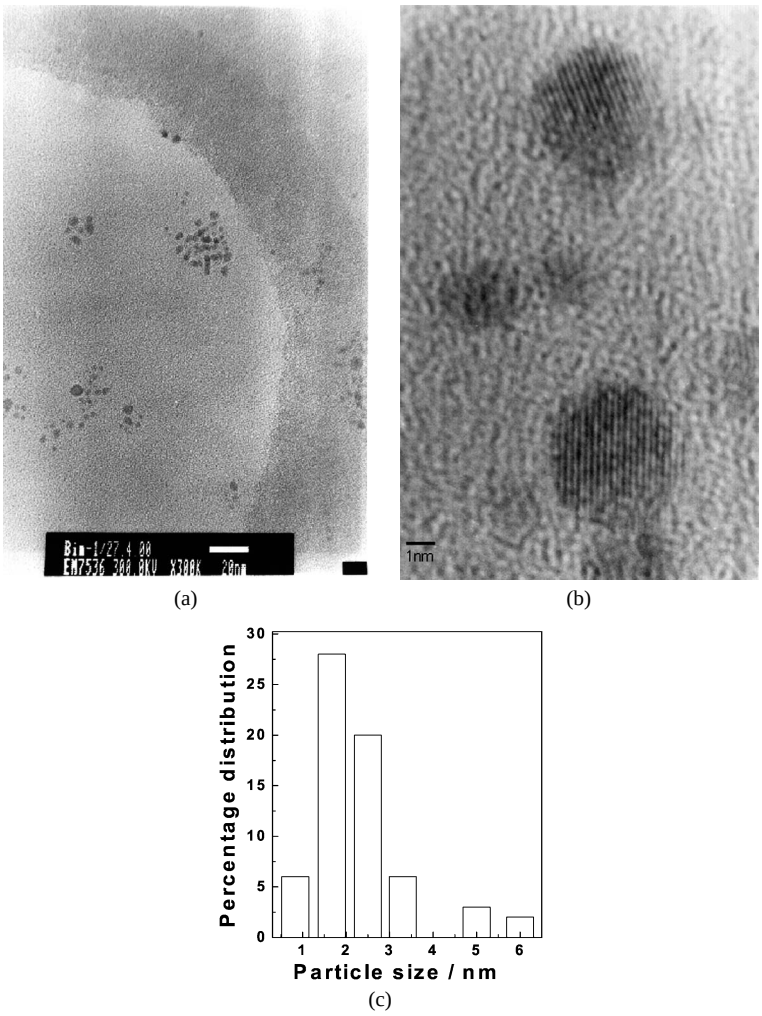

Fig. 6. TEM picture of the TPDT-stabilized Au–Ag bimetallic colloid. The molar ratios of silane to metal salts is 100:5:5. (a) Bar indicates 20 nm; (b) HRTEM image, bar indicates 1 nm; (c) particle size distribution.

due to Pd($3d_{5/2}$) and Au($4d_{5/2}$) core levels that are in close proximity to each other. Accordingly, the spectrum could be deconvoluted into Pd($3d_{5/2,3/2}$) and Au($4d_{5/2}$) peaks. Peaks at 338.1 and 343.1 eV are attributed to Pd($3d_{5/2,3/2}$) spin–orbit doublet peaks indicating that Pd is in a highly ionic Pd^{2+} state, whereas the weak Au($4d_{5/2}$) peak at 336.4 eV corresponding to gold suggests that it is in the zerovalent state.

The surface concentration ratios of Pd to Au at different conditions have been estimated using the relation

$$\frac{C_{\mathrm{Pd}}}{C_{\mathrm{Au}}} = \frac{I_{\mathrm{Pd}}\sigma_{\mathrm{Au}}\lambda_{\mathrm{Au}}D_{\mathrm{E}}(\mathrm{Au})}{I_{\mathrm{Au}}\sigma_{\mathrm{Pd}}\lambda_{\mathrm{Pd}}D_{\mathrm{E}}(\mathrm{Pd})}, \tag{2}$$

where C, I, σ, λ, and D_{E} are the concentration, intensity, photoionization cross-section, mean escape depth, and geometric factor, respectively. Integrated intensities of corresponding metal peaks have been used for the estimation of the concentrations. Photoionization cross-sections and mean escape depths are obtained from the literature [47,48]. The $C_{\mathrm{Pd}}/C_{\mathrm{Au}}$ ratio for Au–Pd after 10 min etching is 1.2, indicating Pd enrichment on the surface. But it decreases to 0.82 and 0.44 after 20 and 30 min etching time. The binding energies of Au and Pd and the $C_{\mathrm{Pd}}/C_{\mathrm{Au}}$ ratios at different etching periods are given in Table 1. This suggests that gold is predominantly in the core of the bimetallic structure and palladium is enriched on the surface. However, it should be noted that the first data point is given only after 10 min of etching.

3.4.2. Au–Pt

The XPS of Au–Pt bimetal does not show any signal for Au($4f$) and Pt($4f$) in the as-prepared samples. Only on etching for 10 min do the peaks become visible. The XPS spectrum of Au($4f$) and Pt($4f$) core level regions after 20 min etching are shown in Fig. 8B. The Au($4f_{7/2,5/2}$) peaks observed at 84.1 and 88.0 eV could be attributed to Au^0. The Pt($4f$) peaks could be resolved into two sets of spin–orbit doublets. Accordingly, Pt($4f_{7/2}$) peaks at 72.8 and 74.2 eV indicate that Pt is present in both 2+ and 4+ oxidation states. The amount of Pt^{2+} is higher than that of Pt^{4+}. After 20 min of etching, Au($4f_{7/2}$) peaks are observed at 83.9 eV whereas Pt($4f_{7/2}$) peaks are observed at 72.6 and

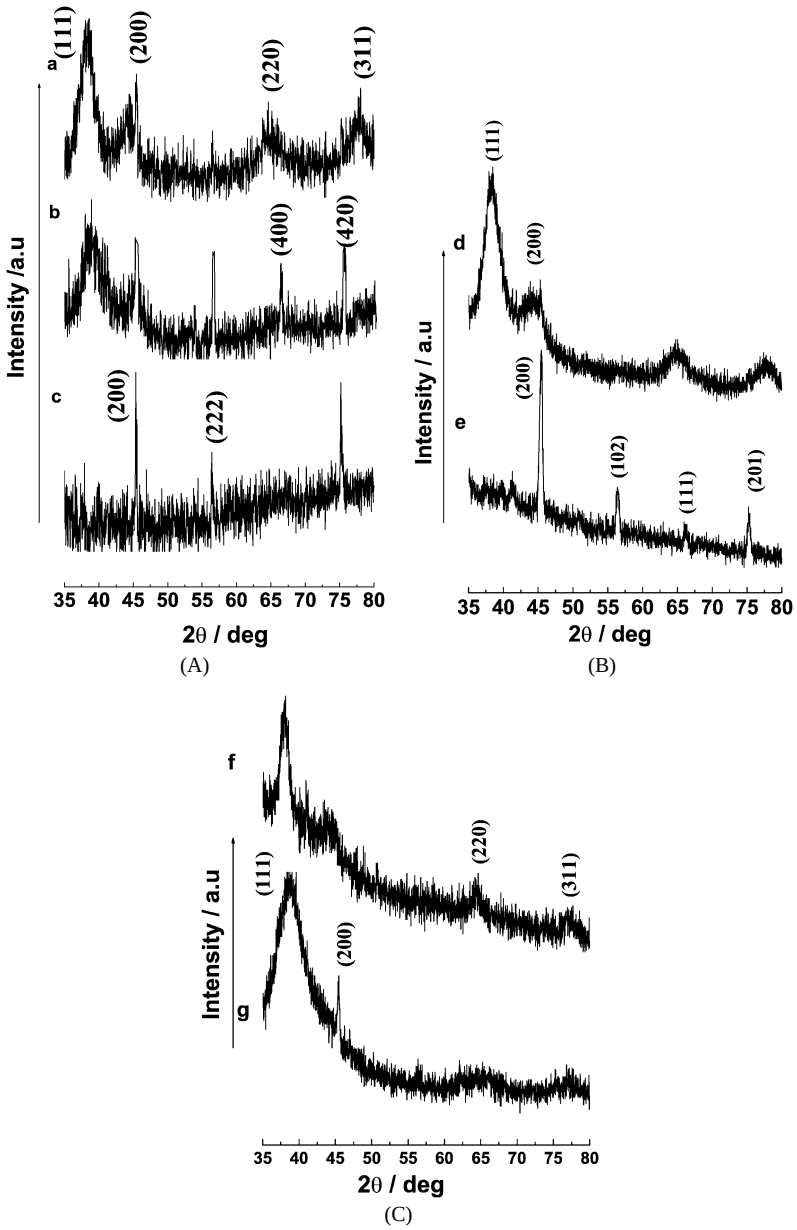

Fig. 7. XRD spectra of TPDT-stabilized metallic colloid for the as-prepared samples. (a) Au; (b) Au–Pd bimetal of molar ratio 0.5:0.5; (c) Pd; (d) Au–Pt of molar ratio 0.5:0.1; (e) Pt; (f) Au–Ag of molar ratio 0.5:0.5; (g) Ag. The molar ratio of the silane to metal salts is 100:5:5 for Au–Pd and Au–Ag and 100:5:1 for Au–Pt.

74.2 eV. The surface concentration ratio C_{Pt}/C_{Au} is 1.05 after 10 min of etching, suggesting a very slight enrichment of Pt, which decreases to 0.42 after 20 min. The binding energies of Au and Pt and C_{Pt}/C_{Au} ratios for different durations of etching are given in Table 2.

3.4.3. Au–Ag

The XPS of Au–Ag shows Au($4f$) and Ag($3d$) peaks at 84.0 and 368.1 eV (Fig. 8C), respectively, showing that the metals are in their zerovalent states. As a function of etching time, the Au($4f$) peak is broadened, indicating that Au is in multiple oxidation states. The Au($4f$) broadens, particularly after about 50 min of etching, and accordingly the Au($4f$) peaks could be deconvoluted into two sets of spin–orbit doublets as Au($4f_{7/2,5/2}$) at 83.9 and 87.7 eV and 85.5 and 89.5 eV corresponding to Au^0 and Au^+ oxidation states, respectively. The relative intensities of Au^0 and Au^+ are 57.5 and 43%, respectively, after 50 min of etching. On the other hand, Ag is in the metallic state even after 75 min of etching. There is no change in the peak position of Ag during etching. The XPS of core level regions of Au($4f$) and Ag($3d$) after 20 min of etching are shown in Fig. 8C. The C_{Ag}/C_{Au} ratio in the as-prepared sample is 11.3, indicating a large enrichment of Ag on the surface. On etching, this ratio decreases, and at etching times of 50 and 75 min, the ratio remains close to 1. Binding energies of Au and Ag and the corresponding ratios of C_{Ag}/C_{Au} at different etching durations are given in Table 3.

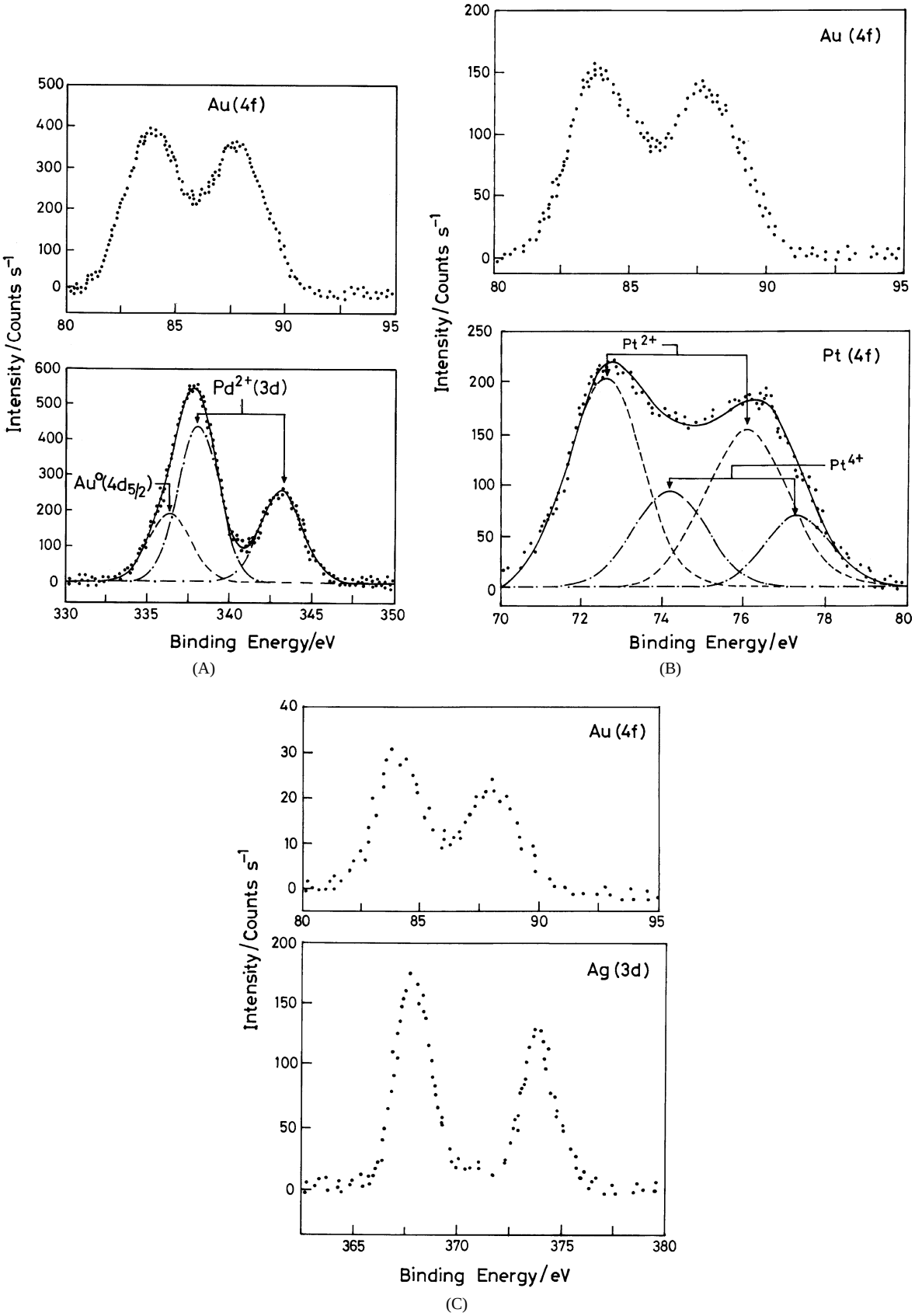

Fig. 8. (A) XPS of core level regions of Au(4*f*) and Pd(3*d*) in silane-protected Au–Pd clusters after 30 min etching. (B) XPS of core level regions of Au(4*f*) and Pt(4*f*) in silane-protected Au–Pt clusters after 30 min etching. (C) XPS of core level regions of Au(4*f*) and Ag(3*d*) in silane-protected Au–Ag clusters after 20 min etching. The molar ratio of the silane to metal salts is 100:5:5 for Au–Pd and Au/Ag and 100:5:1 for Au–Pt.

Table 1
Binding energies (eV) and concentration ratios of Au and Pd species at different etching durations (min)

Duration of etching	Binding energy of Au($4f_{7/2}$)	Binding energy of Pd($3d_{5/2}$)	C_{Pd}/C_{Au}
As prepared	–	–	–
10	83.9	338.1	1.2
20	84.0	338.1	0.82
30	83.9	338.0	0.44

Table 2
Binding energies (eV) and concentration ratios of Au and Pt species at different etching durations (min)

Duration of etching	Binding energy of Au($4f_{7/2}$)	Binding energy of Pt($4f_{7/2}$)	C_{Pt}/C_{Au}
As prepared	–	–	–
10	84.1	72.8 (46%) 74.2 (54%)	1.05
20	83.9	72.6 (70%) 74.2 (30%)	0.42

Table 3
Binding energies (eV) and concentration ratios of Au and Ag species at different etching durations (min)

Duration of etching	Binding energy of Au($4f_{7/2}$)	Binding energy of Ag($3d_{5/2}$)	C_{Ag}/C_{Au}
As prepared	84.0	368.1	11.3
10	84.1	367.9	8.5
20	83.9	368.0	6.7
35	84.0	367.9	4.3
50	83.9 (57%) 85.5 (43%)	368.0	1.2
75	83.9 (56%) 85.5 (44%)	368.1	1.1

3.5. *FT-IR studies*

FT-IR studies have been carried out to follow the evolution of silicate matrix during the stabilization of the metallic particles. The spectra have been taken for the dried material and they represent the completely polymerized silicate network encapsulating the nanoparticles (figure not shown). The IR peaks agree well with the reported literature values [40] for silicate matrices. The band at 1117 cm^{-1} confirms the presence of siloxane groups [γ(Si–O–Si)] in the polymerized material while the band at around 1659 cm^{-1} corresponds to the primary amine [$\delta(NH_2)$] of the silane. The position of this band shifts to higher values as the silane is cross-linked and polymerized. The N–H stretching band around 3500 cm^{-1} is broadened in the cross-linked material as compared to that of neat silane. This is attributed to the complexation of the amine groups of the silicate with the metal particles [40].

3.6. *Carbon monoxide adsorption studies*

Infrared spectroscopy has been widely used to study the surface chemistry of small, adsorbed molecules [49–55]. The vibrational frequency of adsorbed CO changes with the metal substrate and binding structure. Hence, IR spectroscopy of CO on the surface of bimetallic nanoparticles is expected to give information about the surface of the nanoparticle. On gold nanoparticles, however, CO is known to be very weakly and reversibly adsorbed [53,54]. The adsorbed CO is generally observed only at low temperatures [53,54]. Gold and silver have fully occupied d-orbitals ($5d^{10}6s^1$, $4d^{10}5s^1$, respectively) and exhibit weak coordination ability toward CO. It is reported that only weak Raman and IR bands are observed for CO on gold and silver surfaces [53,54]. The IR spectra corresponding to the CO stretching region are given in Fig. 9 for Au–Pd and Au–Pt bimetallic systems. We have earlier reported the CO-IR spectra for monometallic Pd and Pt particles [41,56]. This is similar to the spectra reported by Toshima and coworkers [52].

3.6.1. *Au–Pd*

The IR spectra of CO adsorbed on nanobimetallic 1:1 Au–Pd stabilized in TPDT matrix is shown in Fig. 9a. A broad peak is seen at 2032 cm^{-1} and another strong absorption band is observed at 1911 cm^{-1}. The former band can be assigned to the CO adsorbed on the Pd surface at the terminal site (linear adsorption site) and the latter to CO adsorbed at the bridging site (bridging adsorption site) [52]. The relative intensities of these two peaks have been reported to vary depending on the particle size [49].

3.6.2. *Au–Pt*

The IR spectrum of CO adsorbed on TPDT-stabilized Au–Pt particles is shown in Fig. 9b. A strong band is observed at 2030 cm^{-1} and is assigned to the linearly adsorbed CO on the Pt surface [55].

Hence, in both Au–Pd and Au–Pt bimetallic particles, an enrichment of Pd and Pt is observed on the surface.

3.7. *Electrocatalysis studies*

The electrocatalytic activity of the nanoparticles stabilized in silicate matrices has been followed by carrying out preliminary studies on Au–Pd and Au–Ag alloy nanoparticles. A glassy carbon electrode is coated with the silicate stabilized nanoparticles and used for further experiments. Oxygen reduction is taken as the demonstrative case. Use of TEOS along with TPDT to stabilize the particles facilitates cross-linking and the resulting films are found to be very sturdy and adherent to the substrate. Cyclic voltammetric experiments have been performed on the modified electrode in phosphate buffer pH 7.2. Fig. 10 shows the cyclic voltammograms on the bare as well as nanometal modified electrodes. It is clear that the oxygen reduction potential shifts to more positive values in presence of the metallic particles. A potential shift of about 200 mV in the case of Au–Pd modified classy carbon electrode (Fig. 10a) shows the catalytic nature of the immobilized metallic particles. Similarly, the catalytic

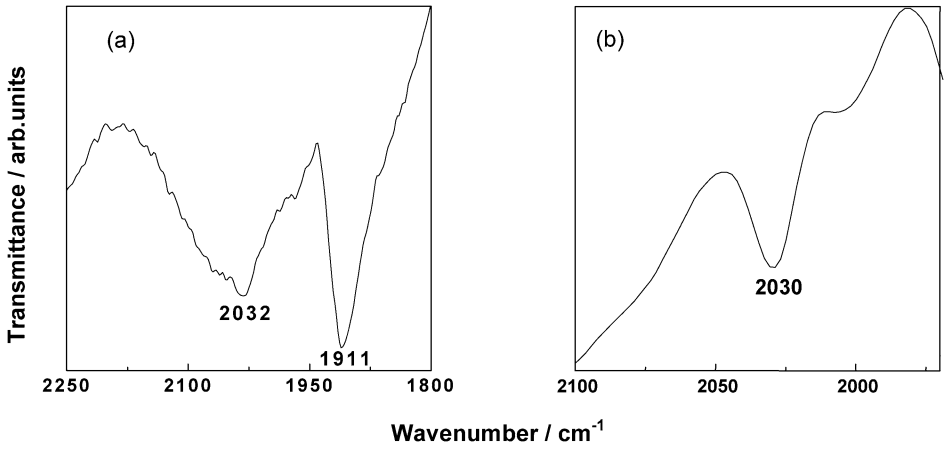

Fig. 9. FT-IR spectra of CO adsorbed on the TPDT-stabilized bimetallic particles. (a) Au–Pd; (b) Au–Pt bimetal. The molar ratios of silane to metal salts are 100:0.5:0.5 and 100:0.5:0.1, respectively.

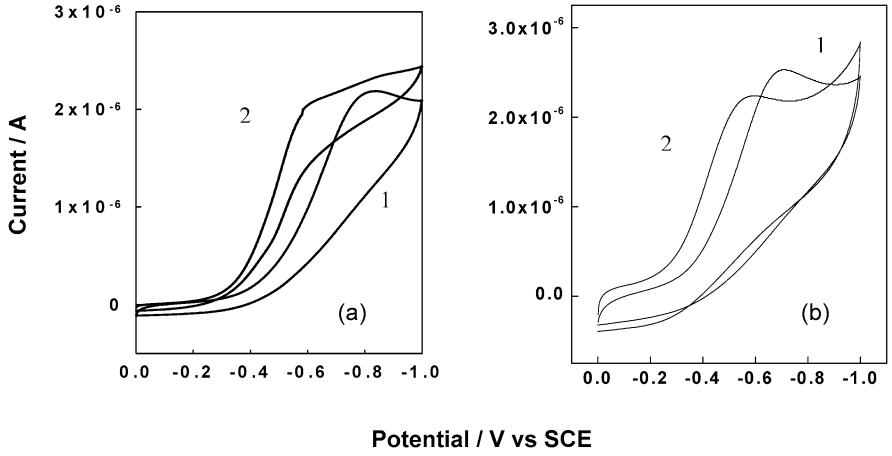

Fig. 10. Cyclic voltammograms of oxygen reduction on a bare- (a1, b1) and nanometal-modified (a2, b2) glassy carbon electrode. Scan rates employed are 5 mV/s. (a) and (b) refer to the Au–Pd bimetal and Au–Ag alloy, respectively. The molar ratio of the silane to metal salts is 100:5:5.

shift in the case of Au–Ag alloy nanoparticles is 150 mV at a scan rate of 5 mV/s (Fig. 10b). Detailed studies are in progress.

4. Conclusions

The preparation of various bimetallic nanoparticles in organically modified silicates has been demonstrated. The studies on Au–Pd and Au–Pt bimetallic particles reveal that the surface consist of both metals while Au–Ag forms alloy phases. The sols remain stable for several months and can be handled and characterized easily. However XRD and XPS measurements carried out on dried samples indicate the formation of oxides. This is expected since sol–gel based silicates are known to be highly porous and permeable to oxygen [57]. The XRD studies also reveal that the nanobimetallic particles predominantly assemble in fcc structure. It should be noted that vapor phase synthesis (solvated metal atom dispersion method) has been reported to lead to nanoparticles assembling in hcp structure [58]. The method employed for the synthesis of the particles seems to play a large role in determining the packing behavior. It appears that fcc ordering in preferred by single crystalline particles while hcp packing is preferred by polycrystalline particles. XRD and TEM measurements for aminosilicate-stabilized bimetallic particles indicate clear single crystalline behavior.

The bimetallic particles prepared by the sol–gel method have been shown to electrocatalyze the reduction of oxygen. The potential applications of these materials in self-assembly, catalysis and surface enhanced Raman spectroscopy are being studied.

Acknowledgments

The authors thank Professor M.S. Hegde, Solid State and Structural Chemistry Unit, Indian Institute of Science, for the XPS studies and Ms. A. Saraswathi for carrying out XRD measurements. Financial support from the Department of Science and Technology (DST) and the Council of Scien-

tific and Industrial Research (CSIR), New Delhi, India, is gratefully acknowledged.

References

[1] N. Toshima, Y. Wang, Chem. Lett. (1993) 1611.
[2] N. Toshima, M. Harada, Y. Yamazaki, K. Asakura, J. Phys. Chem. 96 (1992) 9927.
[3] A.F. Lee, C.J. Baddeley, C. Hardacre, R.M. Ormerod, R.M. Lambert, G. Schmid, H. West, J. Phys. Chem. 99 (1995) 6096.
[4] N. Toshima, M. Harada, T. Yonezawa, K. Kushihashi, K. Asakura, J. Phys. Chem. 95 (1991) 7448.
[5] T. Yonezawa, N. Toshima, J. Mol. Catal. 83 (1993) 167.
[6] J. Turkevich, G. Kim, Science 169 (1970) 873.
[7] Y. Mizukoshi, K. Okitsu, Y. Maeda, T.A. Yamamoto, R. Oshima, Y. Nagata, J. Phys. Chem. 101 (1997) 7033.
[8] Y. Mizukoshi, T. Fujimoto, Y. Nagata, R. Oshima, Y. Maeda, J. Phys. Chem. B 104 (2000) 6028.
[9] G. Schmid, A. Lehnert, J.-O. Malm, J.-O. Bovin, Angew. Chem. Int. Ed. Engl. 30 (1991) 874.
[10] C.J. Baddeley, D.A. Jefferson, R.M. Lambert, R.M. Ormerod, T. Rayment, G. Schmid, A.P. Walker, Mater. Res. Soc. Symp. Proc. 272 (1992) 85.
[11] R.J. Davis, M. Boudart, J. Phys. Chem. 98 (1994) 5471.
[12] B. Helmut, U. Endruschat, B. Tesche, A. Rufinska, C.W. Lehmann, F.E. Wagner, G. Filoti, V. Parvulescu, V.I. Parvulescu, Eur. J. Inorg. Chem. 5 (2000) 819.
[13] M. Harada, K. Asakura, N. Toshima, J. Phys. Chem. 97 (1993) 5103.
[14] T. Yonezawa, N. Toshima, J. Chem. Soc. Faraday Trans. 91 (1995) 4111.
[15] N. Toshima, T. Yonezawa, New J. Chem. 22 (1998) 1179.
[16] N. Toshima, M. Harada, Y. Yamazaki, K. Asakura, J. Phys. Chem. 96 (1992) 9927.
[17] H. Liu, G. Mao, M. Meng, J. Mol. Catal. 74 (1992) 2775.
[18] L. Guczi, A. Beck, A. Horvath, Zs. Koppany, G. Stefler, K. Frey, I. Sajo, D. Bazin, J. Lynch, J. Mol. Catal. A Chem. 204–205 (2003) 545.
[19] N.T. Flynn, A.A. Gewirth, J. Raman Spectrosc. 33 (2002) 243.
[20] T. Takenaka, K. Eda, J. Colloid Interface Sci. 105 (1985) 342.
[21] H. Tada, F. Suzuki, S. Ito, T. Akita, K. Tanaka, T. Kawahara, H. Kobayashi, J. Phys. Chem. B 106 (2002) 8714.
[22] C. Mihut, C. Descorme, D. Duprez, M.D. Amirdis, J. Catal. 212 (2002) 125.
[23] L.M. Liz-Marzan, A.P. Philipse, J. Phys. Chem. 99 (1995) 15,120.
[24] P. Mulvaney, M. Giersig, A. Henglein, J. Phys. Chem. 97 (1993) 7061.
[25] R.G. Freeman, M.B. Hommer, K.C. Grabar, M.A. Jackson, M.J. Natan, J. Phys. Chem. 100 (1996) 718.
[26] I. Srnova-Sloufova, F. Lednicky, A. Gemperle, J. Gemperlova, Langmuir 16 (2000) 9928.
[27] G.C. Papavassiliou, J. Phys. F Met. Phys. 6 (1976) L103.
[28] N. Aihara, K. Torigoe, K. Esumi, Langmuir 14 (1998) 4945.
[29] H.Z. Shi, L.D. Zhang, W.P. Cai, J. Appl. Phys. 87 (2000) 1572.
[30] M.J. Hostetler, C.J. Zhong, B.K. Yen, J.H. Anderegg, S.M. Gross, N.D. Evans, M. Porter, R.W. Murray, J. Am. Chem. Soc. 120 (1998) 9396.
[31] N. Sandhyarani, T. Pradeep, Chem. Mater. 12 (2000) 1755.
[32] J. Sinzig, U. Radtke, M. Quinten, U. Kreibig, Z. Phys. D 26 (1993) 242.
[33] B.K. Teo, K. Keating, Y.H. Kao, J. Am. Chem. Soc. 109 (1987) 3494.
[34] D.-H. Chen, C.-J. Chen, J. Mater. Chem. 12 (2002) 1557.
[35] M.P. Mallin, C.J. Murphy, Nano Lett. 2 (2002) 1235.
[36] M. Brust, M. Walker, D. Bethell, D.J. Schiffrin, R. Whyman, J. Chem. Soc. Chem. Commun. (1994) 801.
[37] M. Brust, J. Fink, D. Bethell, D.J. Schiffrin, C. Kiely, J. Chem. Soc. Chem. Commun. (1995) 1655.
[38] S. Link, Z.L. Wang, M.A. El-Sayed, J. Phys. Chem. B 103 (1999) 3529.
[39] S. Devarajan, B. Vimalan, S. Sampath, J. Colloid Interface Sci. 278 (2004) 126.
[40] S. Bharathi, N. Fishelson, O. Lev, Langmuir 15 (1999) 1929.
[41] L. D'Souza, S. Sampath, Langmuir 16 (2000) 8510.
[42] J.A. Creighton, D.G. Eadon, J. Chem. Soc. Faraday Trans. 87 (1991) 3881.
[43] L.G. Sillen, A.E. Martell, Stability Constants of Metal-Ion Complexes, Special Publication No. 17, The Chemical Society, London, 1964.
[44] R.M. Smith, A.E. Martell, Critical Stability Constants: Amines, vol. 2, Plenum, New York, 1975.
[45] N. Toreis, X.E. Verykios, S.M. Khalid, G.B. Bunker, Surf. Sci. 197 (1988) 415.
[46] L.M. Liz-Marzan, M. Giersig, P. Mulvaney, Langmuir 12 (1996) 4329.
[47] J.H. Scofield, J. Electron Spectrosc. Relat. Phenom. 8 (1976) 129.
[48] D.R. Penn, J. Electron Spectrosc. Relat. Phenom. 9 (1976) 29.
[49] J.S. Bradley, E.W. Hill, S. Behal, C. Klein, B. Chaudret, A. Duteil, Chem. Mater. 4 (1992) 1234.
[50] J.S. Bradley, J.M. Millar, E.W. Hill, S. Behal, B. Chaudret, A. Duteil, Faraday Discuss. Chem. Soc. 92 (1991) 255.
[51] J.S. Bradley, in: G. Schmid (Ed.), Clusters and Colloids, VCH, Weinheim, 1994, pp. 459–544.
[52] Y. Wang, N. Toshima, J. Phys. Chem. B 101 (1997) 5301.
[53] S.-G. Sun, W.-B. Cai, L.-J. Wan, M. Osawa, J. Phys. Chem. B 103 (1999) 2460.
[54] A.M. Bradshaw, J. Pritchard, Proc. Roy. Soc. London Ser. A 316 (1970) 169.
[55] K.A. Friedrich, F. Henglein, U. Stimming, W. Unkauf, Electrochim. Acta 47 (2001) 689.
[56] L. D'Souza, P. Bera, S. Sampath, J. Colloid Interface Sci. 246 (2002) 92.
[57] C.J. Brinker, G.W. Scherer, Sol–Gel Science—The Physics and Chemistry of Sol–Gel Processing, Academic Press, New York, 1990.
[58] S.I. Stoeva, B.L.V. Prasad, S. Uma, P.K. Stoimenov, V. Zaikovski, C. Sorensen, K.J. Klabunde, J. Phys. Chem. B 107 (2003) 7441.